Supplementary Information

for

Quasi-1D/3D Bi_2O_4/Phase-tuned C_3N_5 Type-II heterostructure for the visible-light-driven photocatalytic degradation of resorcinol in wastewater: Insights into inhibitory effects of matrix interferences and phytotoxicity assessment

Adarsh Singh [a], Balbir [a], Suneel Kumar Srivastava [b#], Amit Bhatnagar [c], Ashok Kumar Gupta [a*]

[a] Environmental Engineering Division, Department of Civil Engineering,

Indian Institute of Technology Kharagpur, Kharagpur 721302, India

[b] Department of Chemistry,

Indian Institute of Technology Kharagpur, Kharagpur 721302, India

[#] Retired Professor

[c] Department of Separation Science, LUT School of Engineering Science,

LUT University, Sammonkatu 12, Mikkeli FI-50130, Finland

* Corresponding author.

E-mail address: agupta@civil.iitkgp.ac.in (A. K. Gupta)

Section S1 Procedure for seed germination assay

As previously reported, *Vigna radiata* seeds were chosen as a representative species in order to measure phytotoxicity.[1–5] The seeds were submerged in deionized (DI) water for 12 h to evaluate their viability. For the experiment, the tissue soaked separately in DI water, an untreated sample containing 5 mg/L of RCL, and a sample that had been photocatalytically treated were all placed into different beakers. Using tweezers, 20 *Vigna radiata* seeds were carefully placed in each beaker, leaving enough space between them. The beakers were then incubated for five days at 28 °C. Following five days of incubation, the length of the seedling was assessed using the thread. The seed germination index (GI) was calculated using the following Eq. S1:[6]

$$GI\ (\%) = [\text{Relative seed germination (RSG)} \times \text{Relative radicle growth (RRG)}] \times 100 \qquad (S1)$$

where, RSG can be denoted as the ratio of seeds germinated in a sample to those in the control, while RRG can be denoted as the average radicle length in the sample to that in the control. The sample can be categorized as highly phytotoxic (GI < 50%), moderately phytotoxic (50% < GI < 80%), or non-phytotoxic (GI > 80%) based on its GI value.

Section S2 Liquid chromatography and tandem mass spectrometry (LC-MS/MS)

LC-MS/MS analyses were performed on a Waters 2695 quaternary HPLC system (quaternary pump, online vacuum degasser, autosampler, and thermostatic column compartment) coupled in-line to a photodiode array detector (Waters 2998) and a QuattroMicro™ API triple quadrupole mass spectrometer (Waters, Milford, MA, USA). The data acquisition and analysis were conducted using MASS LYNX 4.1 software (Waters). A sample of 10 µL was injected into the system using an autosampler, and chromatographic separations were done on an XTerra MS C18 reversed-phase column (21 x 100 mm i.d., 25 µm particle size; Waters). The mobile phase

comprised 70% of eluent A and 30% of eluent B over 10 min [Eluent A: water/formic acid (0.1 v/v%); and eluent B: acetonitrile/formic acid (0.1 v/v%)]. The flow rate was 0.3 mL/min, and the column temperature was maintained at 25 ^{o}C. The parent compound and the intermediates were identified using a PDA detector set at wavelength 272 nm. The LC effluent was directed to the MS via a post-column split (3:1) into an electrospray ionization source operated in positive mode (ES^{+}) (source block temperature: 130 ^{o}C, desolvation temperature: 300 ^{o}C, capillary voltage: 3.0 kV, cone voltage: 30 V). The desolvation and cone gas flows were 450 and 80 L/h, respectively. Data were acquired in MS scan mode with a scan time of 0.5 s and an interscan delay of 0.1 s.

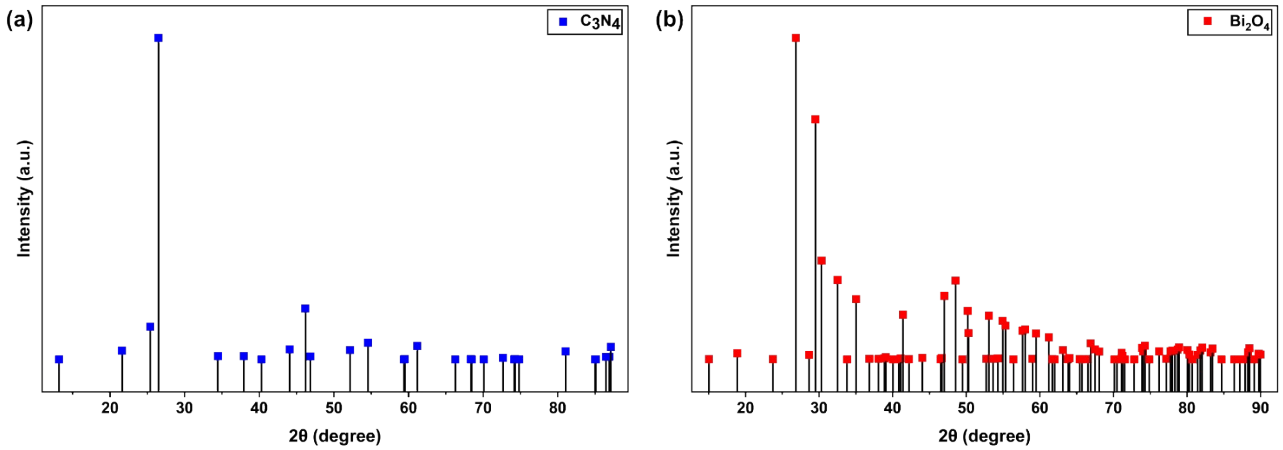

Fig. S1 JCPDS spectra of pristine (a) C_3N_4 (JCPDS No. 87-1526), and (b) Bi_2O_4 (JCPDS No. 83-0410).

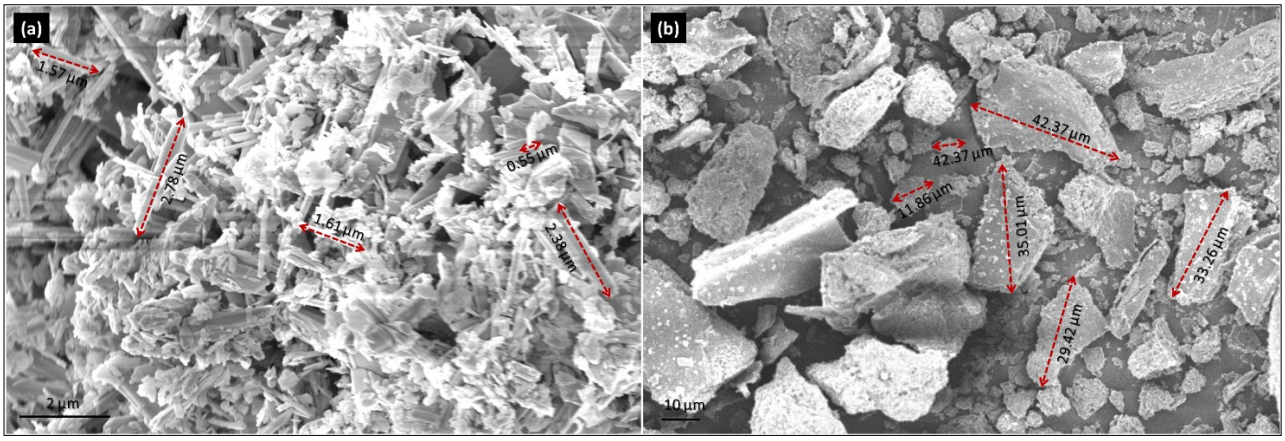

Fig. S2 Particle size of (a) Bi_2O_4, and (b) PT-C_3N_5.

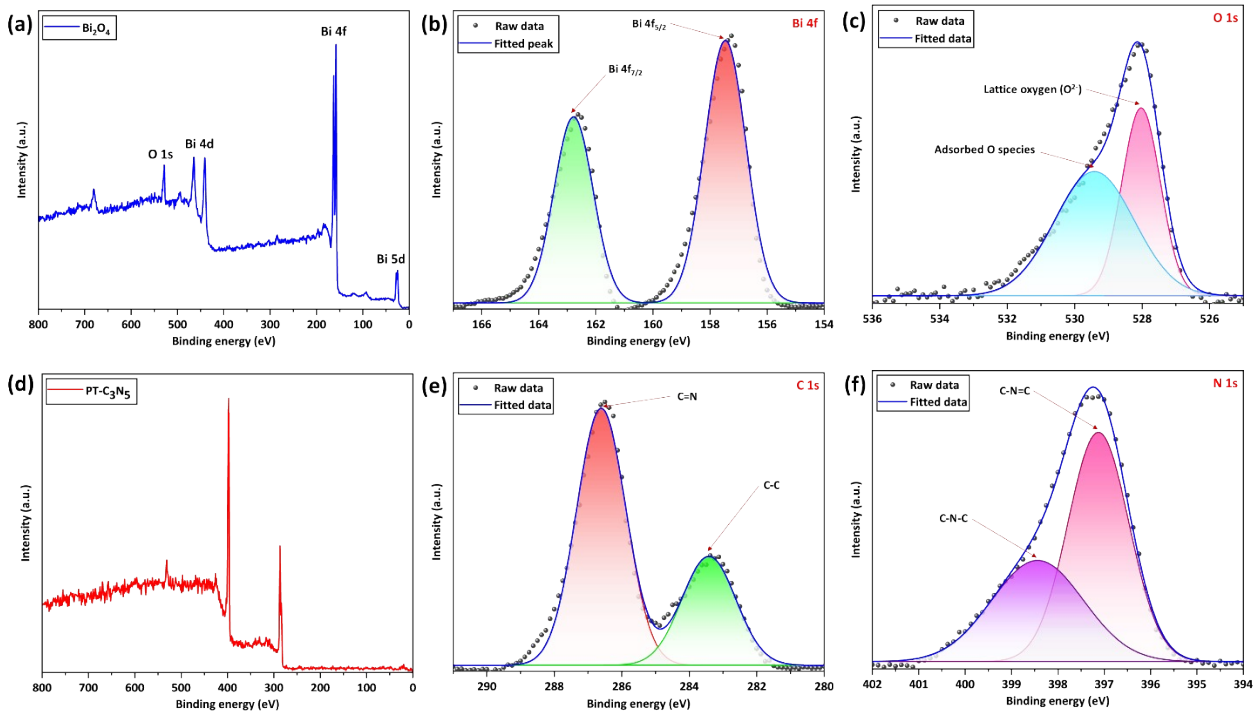

Fig. S3 (a) Full XPS survey scan spectrum of Bi_2O_4, high resolution XPS spectrum of (b) Bi 4f (157.5 eV [7], 162.8 eV [7]) (c) O 1s (529.4 eV [8], 528.1 eV [9]). (d) Full XPS survey scan spectrum of PT-C_3N_5, high resolution XPS spectrum of (b) C 1s (283.4 eV [10], 286.6 eV [11]), (c) N 1s (397.1 eV [12], 398.4 eV [13]).

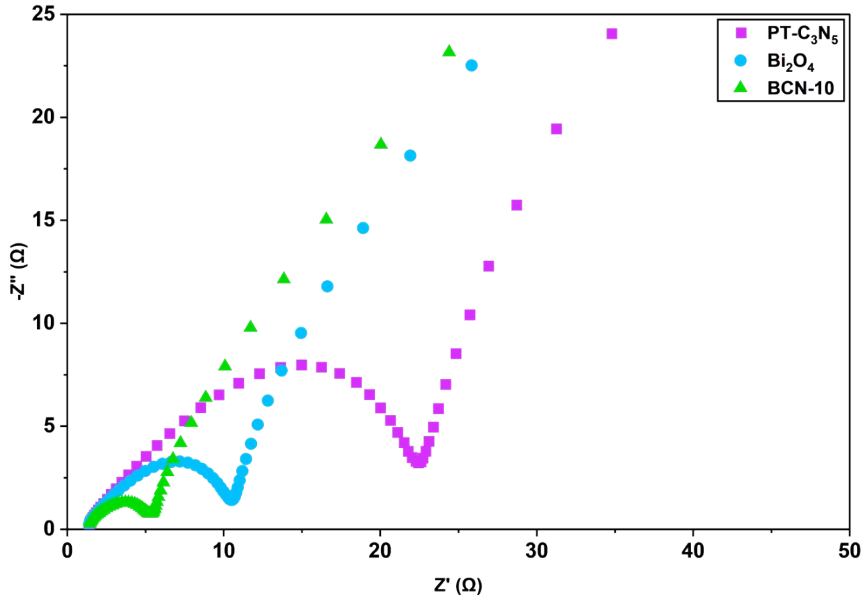

Fig. S4 Electrochemical impedance spectroscopy (EIS) plot of the as-synthesized PT-C_3N_5, Bi_2O_4, and BCN-10.

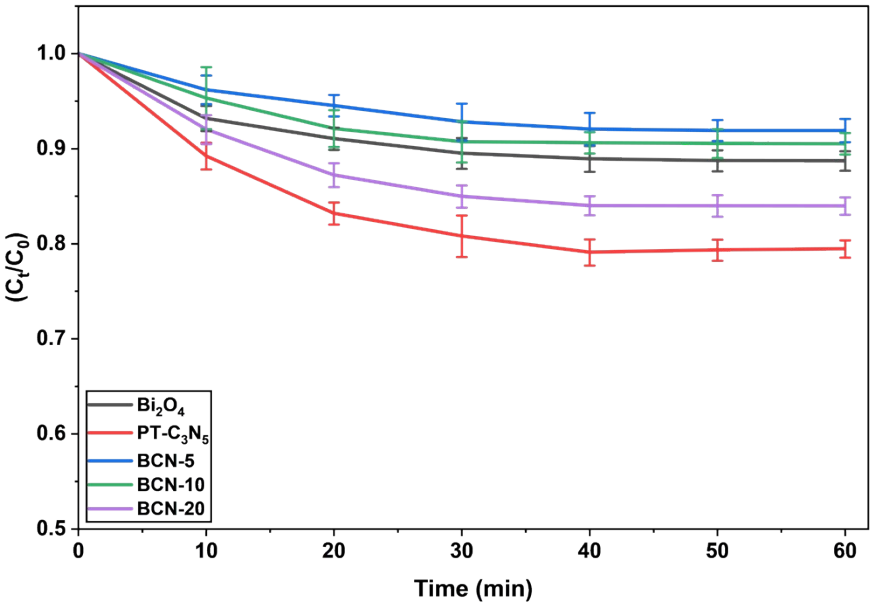

Fig. S5 Adsorptive removal of RCL using BCN-10 in dark.

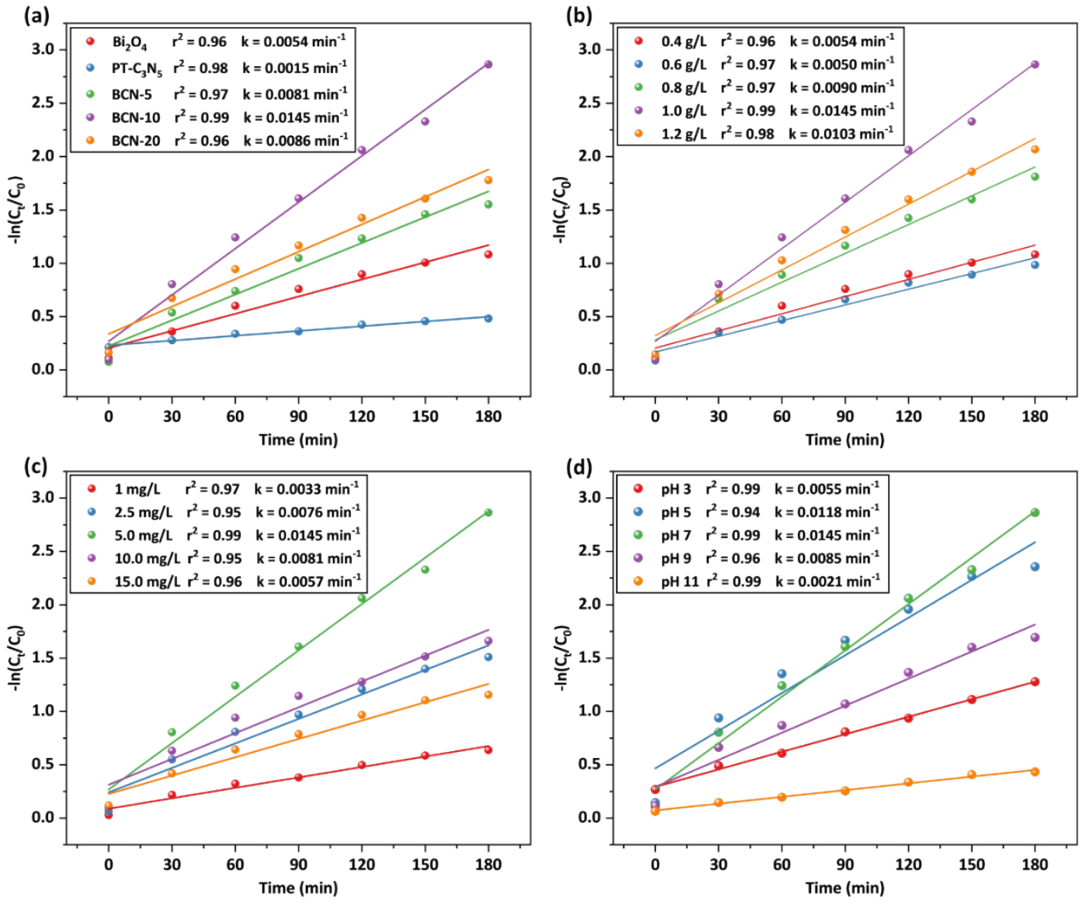

Fig. S6 Pseudo-first-order degradation kinetics plots for RCL using pristine and composite photocatalysts under various reaction conditions.

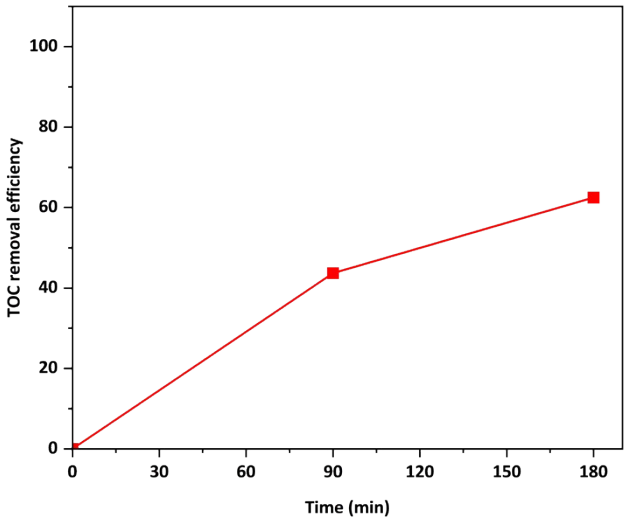

Fig. S7 Mineralization efficiency of BCN-10 photocatalyst for RCL.

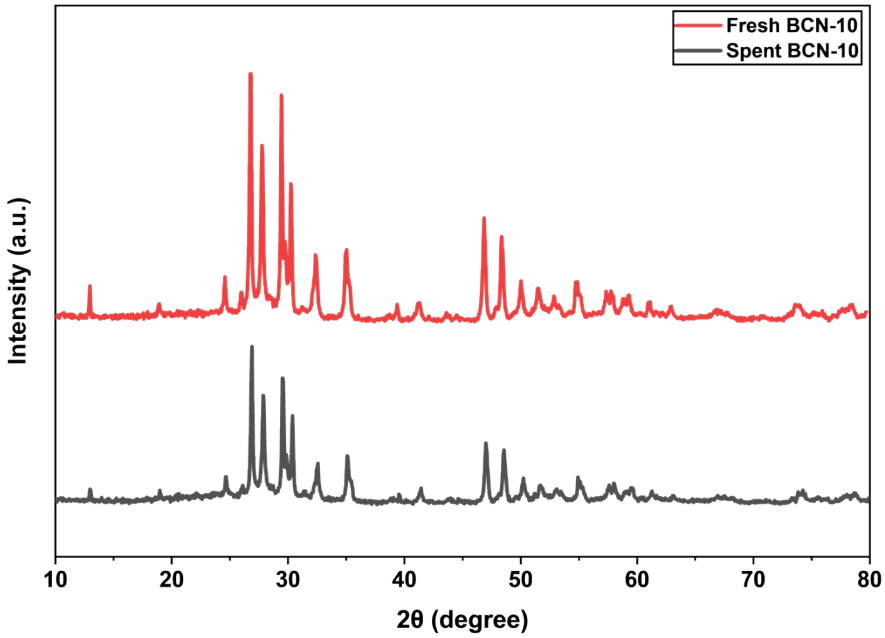

Fig. S8 XRD spectra of (a) fresh , and (b) spent BCN-10 photocatalysts.

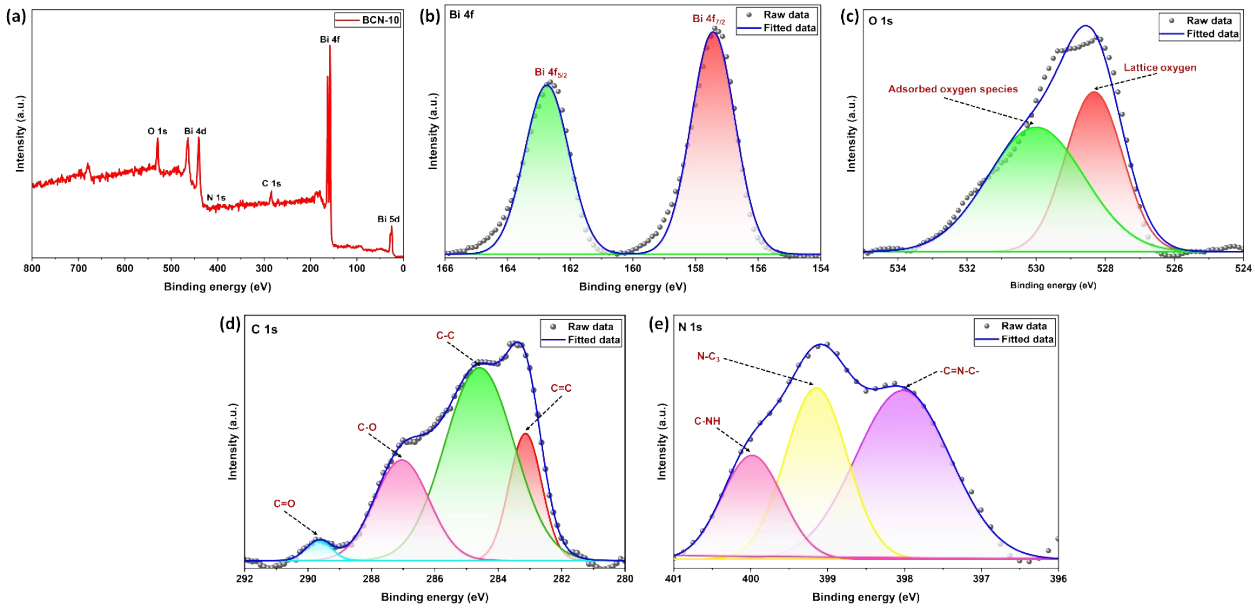

Fig. S9 (a) Full survey scan XPS spectrum of spent BCN-10. High resolution XPS spectrum of (b) Bi 4f (162.75 eV, 157.43 eV) (c) O 1s (530 eV[14], 528.32 eV[15]) (d) C 1s (289.65 eV[16], 287.02 eV[16], 284.59 eV[17], 283.13 eV[18]) and (e) N 1s (399.98 eV[19], 399.14 eV[20], 398.02 eV[19]).

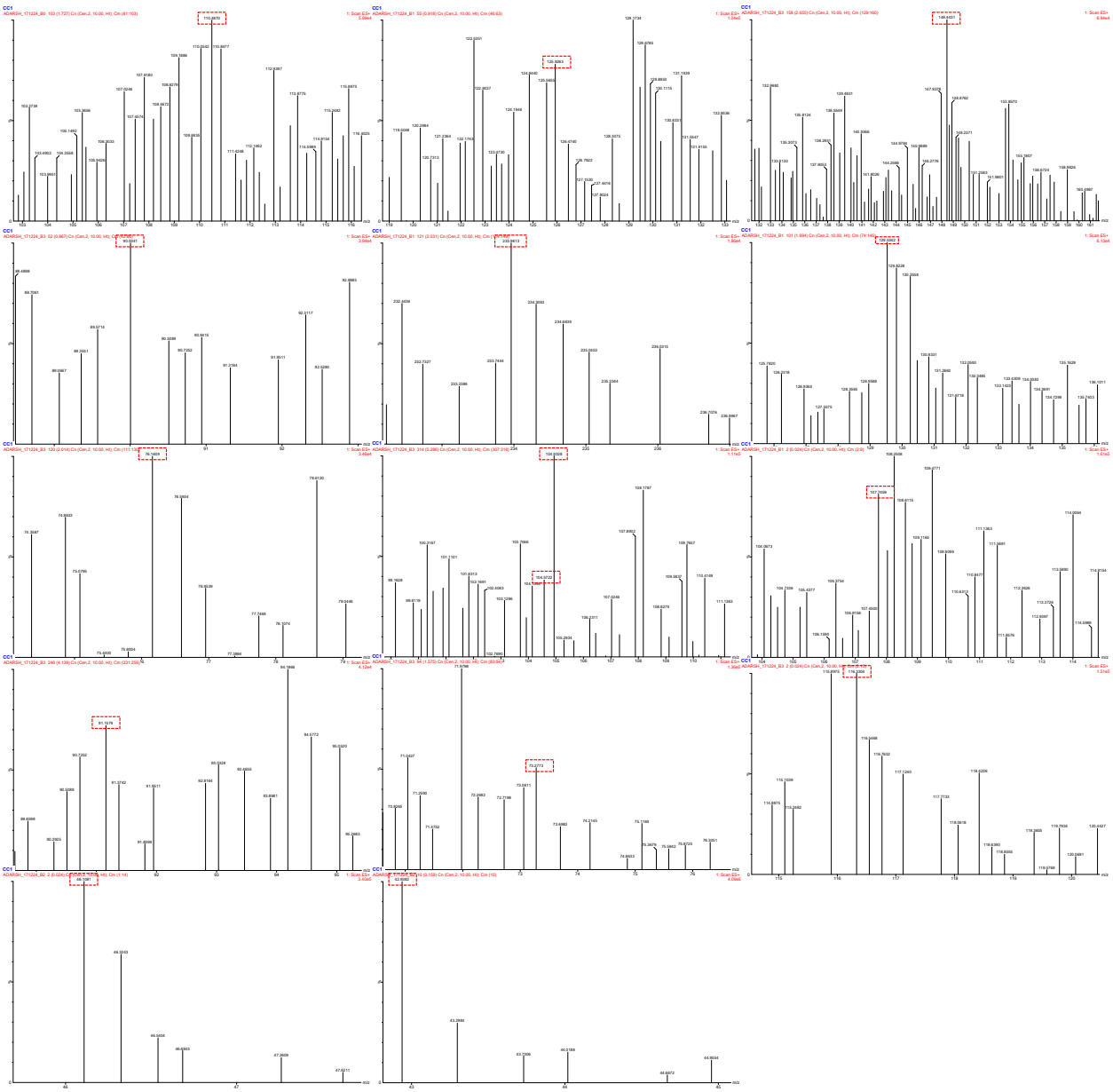

Fig. S10 Transformation products (TPs) of RCL identified from LC-MS/MS analysis.

Table S1 Detailed information about the chemicals used in this study.

S.no.	Chemical	Purity	Use	Source
1.	3-amino-1,2,4-triazole ($C_2H_4N_4$)	>98%	Heterojunction synthesis	Merck, India
2.	Sodium bismuthate ($NaBiO_3$)	80%		
3.	Ethanol (C_2H_5OH)	≥ 99.9%		
4.	Sodium Chloride (NaCl)	≥ 99.5%	Study the influence of co-existing anions	
5.	Sodium sulfate anhydrous (Na_2SO_4)	≥ 99%		
6.	Sodium nitrate ($NaNO_3$)	≥ 99.9%		
7.	Sodium carbonate ($NaHCO_3$)	≥ 99.5%		
8.	Potassium iodide (KI)	≥ 99%	Radical scavenging studies	
9.	Isopropyl alcohol (C_3H_8O)	99%		
10.	Humic acid ($C_9H_9NO_6$)	≥99%		
11.	Ascorbic acid ($C_6H_8O_6$)	≥ 99.9%		
12.	Resorcinol ($C_6H_6O_2$)	99%	Photocatalytic degradation	
13.	Levofloxacin ($C_{18}H_{20}FN_3O_4$)	99%		
14.	Bisphenol A ($(CH_3)_2C(C_6H_4OH)_2$)	≥ 99%		
15.	Methylene blue (MB) dye	C.I. 52015		
16.	Deionized (DI) water (H_2O)	-	Solvent and washing	
17.	Sodium hydroxide (NaOH)	≥ 99%	pH adjustment	
18.	Hydrochloric acid (HCl)	35%		

Table S2 Instruments used in the characterization and analysis.

S. No.	Characterization and Analysis Method	Instrument/ Manufacturer	Objective
1	X-ray diffraction (XRD) analysis	D2 Phaser, Bruker, USA	To examine the crystal structure

2	Fourier-transform infrared spectroscopy (FTIR)	Bruker Alpha II	To determine functional groups and chemical composition
3	Field emission scanning electron microscopy (FEG-SEM) Energy dispersive X-ray spectroscopy (EDS)	Zeiss Merlin Gemini II, Germany	To examine surface morphology and elemental composition
4	Atomic force microscopy (AFM)	Agilent 5500 Atomic Force Microscope	To study surface topography
5	X-ray Photoelectron Spectroscopy (XPS)	PHI 5000 VersaProbe III, ULVAC PHI Inc., USA	To investigate surface chemical states
6	UV-Vis diffuse reflectance spectroscopy	Cary 5000 UV-Vis-NIR spectrophotometer	To examine optical properties
7	Inductively coupled plasma optical emission spectroscopy (ICP-OES)	iCAP PRO, Thermo Scientific, USA	To evaluate metal leaching
8	Thermo-gravimetric and Differential Thermal Analysis (TGA-DTA)	Perkin Elmer Pyris Diamond	To examine thermal stability and decomposition kinetics
9	Liquid chromatography-mass spectrometry (LC-MS)	Quattro micro™ API, Waters, USA	To identify transformation products
10	Spectrophotometer	Cary 60 UV-Vis Spectrophotometer	To quantify the concentration of aliquots
11	CHNS-O analyzer	Euro EA CHNSO Analyzer	To determine the chemical composition
12	High-resolution transmission electron microscopy (HRTEM)	JEOL (JEM-ARM300F2) (Double Aberration-corrected 300 kV HRTEM)	To perform high-resolution imaging and elemental mapping of the photocatalyst
13	Pulsed Electron paramagnetic resonance (EPR) Spectrometer (X-band)	Bruker (ELEXSYS 580)	To detect active species involved in photocatalytic

			degradation

Table S3 Textural properties of Bi_2O_4, PT-C_3N_5, and BCN-10 photocatalysts, as obtained by BET and BJH analysis.

Photocatalyst	**BET surface area (m^2/g)**	**Cumulative pore volume (cm^3/g)**	**Average pore size (diameter, nm)**
Bi_2O_4	2.865	0.002	3.1276
PT-C_3N_5	1.034	0.001	3.4876
BCN-10	1.469	0.001	3.1260

Table S4 Comparison of BCN-10 photocatalyst with previously reported photocatalysts for RCL degradation.

Photocatalyst	**Light source**	**Initial RCL concentration**	**Catalyst dosage**	**pH**	**Strategies**	**Degradation efficiency**	**References**
$NiFe_2O_4/CuInSe_2$	300 W Xenon lamp ($\lambda > 420$ nm)	10 mg/L	1.07 g/L	-	Type-II heterojunction	95% (120 min)	[21]
Au/TiO_2	365W UVA lamp	10 mg/L	1 g/L	-	Surface plasmon resonance	95.34% (300 min)	[22]
Bismuth oxybromide/oxyiodide ($Bi_4O_5Br_xI_{2-x}$)	500 W Xenon lamp ($\lambda > 420$ nm)	30 mg/L	1 g/L	-	Defect engineering	92% (180 min)	[23]
ZnO@BiOX	300 W Xenon lamp ($\lambda > 420$ nm)	30 mg/L	1 g/L	-	Z-scheme heterojunction	100% (250 min)	[24]

Bi_2O_3-Nanoparticle/$Bi_4O_5Br_2$	400 W Xenon lamp ($\lambda > 420$ nm)	30 mg/L	1 g/L	7.2	Type-II heterojunction	97% (300 min)	[25]
Bi_2MoO_6/In(OH)$_3$	500 W Xenon lamp ($\lambda > 420$ nm)	20 mg/L	1 g/L		Heterojunction	50% (15 h)	[26]
NT-TiO_2	500 W Xenon lamp ($\lambda > 420$ nm)	10 mg/L	0.5 g/L	-	Doped multiphasic heterojunction	48.5% (120 min)	[27]
Ag_2O/ZnO	55 W CFL	20 mg/L	1 g/L	-	Hetrojunction	100% (360 min)	[28]
N-doped TiO_2 NRs	UV lamp mercury (300 W); Xenon arc lamp ($\lambda > 420$ nm)	100 mg/L	1 g/L	-	Doping	100% (95 min); 100% (85 min)	[29]
TiO_2 nanowire	Xe arc lamp	20 mg/L	1 g/L	-	-	98.4% (180 min)	[30]
TiO_2 nanoparticles	Xe arc lamp	20 mg/L	1 g/L	-	-	98.7% (180 min)	[30]
TiO_2-P25(commercial)	Xe arc lamp	20 mg/L	1 g/L	-	-	83% (180 min)	[30]
BCN-10	**50 W LED light ($\lambda > 420$ nm)**	**5 mg/L**	**1 g/L**	**7**	**Type-II heterojunction**	**94.3% (180 min)**	**Present work**

Table S5 Water quality parameters of various water matrices.

Parameters	**DI water**	**Surface water**	**Secondary wastewater**
pH	6.58±0.2	6.41±0.3	6.62±0.1
Turbidity (NTU)	0.3±0.1	10.6±0.1	18.8±3.1
TSS (mg/L)	-	43±8	61±5

TDS (mg/L)	-	133±8	287±4
Chloride (Cl^-, mg/L)	0.27±0.01	18.5±2.4	73.21±4.6
Sulfate (SO_4^{2-}, mg/L)	-	-	11±0.8
Nitrate (NO_3^-, mg/L)	-	28.5±2.4	68±2.7
Phosphate (PO_4^{3-}, mg/L)	-	6.4±0.9	15.16±1.3
COD (mg/L) [spiked with RCL: 5 mg/L]	-	88±4.5	139.66±5.7

Table S6 TPs of RCL identified through HPLC-MS/MS analysis. (Source: Fig. S10)

Compound	m/z value	Chemical Structure
RCL	110.49	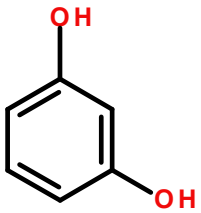
TP1	125.93	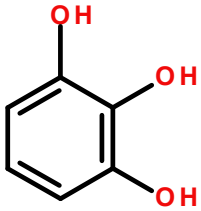
TP2	148.44	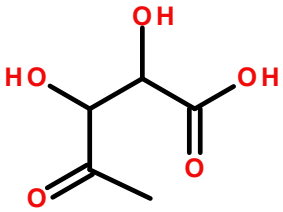
TP3	90.00	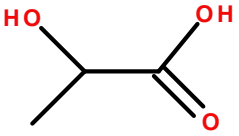

TP4	42.94	
TP5	233.96	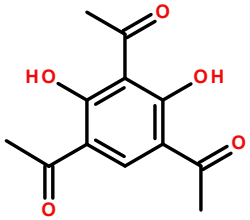
TP6	129.53	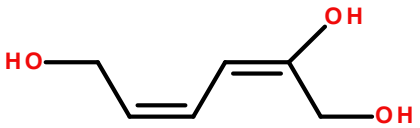
TP7	76.16	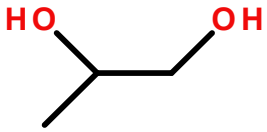
TP8	104.93	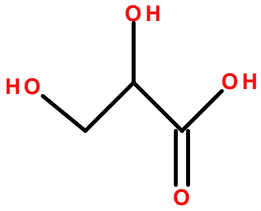
TP9	104.57	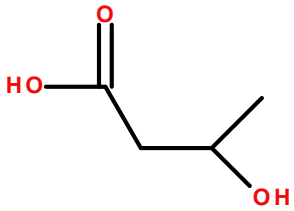
TP10	107.74	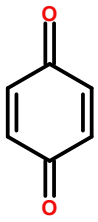
TP11	91.16	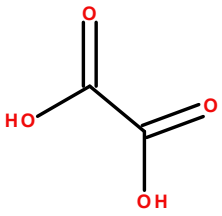

TP12	73.27	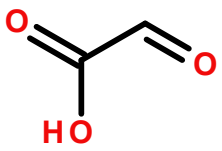
TP13	46.11	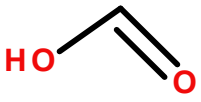
TP14	116.33	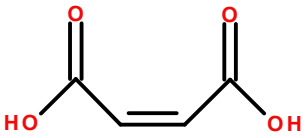

References

1 C. Sakthivel, A. Nivetha, G. Thiruppathi, P. Sundararaj and I. Prabha, *New Journal of Chemistry*, 2023, **47**, 571–588.

2 G. Shukla, M. Rani and U. Shanker, *Inorganic Chemistry Communications*, 2025, **179**, 114733.

3 K.-L. Lim, J.-C. Sin, S.-M. Lam, H. Zeng, H. Lin, H. Li, L. Huang, A. R. Mohamed and J.-W. Lim, *Inorganic Chemistry Communications*, 2025, **174**, 114063.

4 T. Thinley, J. S. Prabagar, S. Yadav, H. S. Anusha, K. M. Anilkumar, W. Kitirote, B. Shahmoradi and H. P. Shivaraju, *Journal of Molecular Structure*, 2023, **1285**, 135413.

5 C. Chokejaroenrat, C. Sakulthaew, A. Angkaew, A. Pattanateeradetch, W. Raksajit, K. Teingtham, P. Phansak, P. Klongvessa, D. D. Snow, C. E. Harris and S. D. Comfort, *Antibiotics*, 2023, **12**, 1151.

6 E. R. Emino and P. R. Warman, *Compost Science & Utilization*, 2004, **12**, 342–348.

7 S. Deka, M. B. Devi, M. R. Khan, Keerthana, A. Venimadhav and B. Choudhury, *ACS Applied Nano Materials*, 2022, **5**, 10724–10734.

8 V. D. Mote, S. D. Lokhande, L. H. Kathwate, M. B. Awale and Y. Sudake, *Materials Science and Engineering: B*, 2023, **289**, 116254.

9 J.-I. Jung and D. D. Edwards, *Journal of Solid State Chemistry*, 2011, **184**, 2238–2243.

10 S. Gu, G. Du, Y. Su, Y. Zhang, Y. Zhang, L. Li, H. Pang and H. Zhou, *Journal of Colloid and Interface Science*, 2025, **677**, 21–29.

11 A. Kumar, A. Kumari, G. Sharma, B. Du, M. Naushad and F. J. Stadler, *Journal of Molecular Liquids*, 2020, **300**, 112356.

12 Z. Lu, C. Li, J. Han, L. Wang, S. Wang, L. Ni and Y. Wang, *Applied Catalysis B: Environmental*, 2018, **237**, 919–926.

13 N. A. Mohamed, J. Safaei, A. F. Ismail, M. F. A. M. Jailani, M. N. Khalid, M. F. M. Noh, A. Aadenan, S. N. S. Nasir, J. S. Sagu and M. A. M. Teridi, *Applied Surface Science*, 2019, **489**, 92–100.

14 T. E. Jones, T. C. R. Rocha, A. Knop-Gericke, C. Stampfl, R. Schlögl and S. Piccinin, *ACS Catalysis*, 2015, **5**, 5846–5850.

15 Y. Kim, H. Schlegl, K. Kim, J. T. S. Irvine and J. H. Kim, *Applied Surface Science*, 2014, **288**, 695–701.

16 M. B. M. Roshtkhari and M. H. Entezari, *Environmental Science and Pollution Research*, 2024, **31**, 15105–15125.

17 D. Gao, Y. Liu, P. Liu, M. Si and D. Xue, *Scientific Reports*, 2016, **6**, 35768.

18 M. Benamara, S. S. Teixeira, M. P. F. Graça, M. A. Valente, S. K. Jakka, H. Dahman, E. Dhahri, L. El Mir, M. Debliquy and D. Lahem, *Applied Physics A*, 2021, **127**, 706.

19 F. Tang, J. Hou, K. Liang, J. Huang and Y. Liu, *European Journal of Inorganic Chemistry*, 2018, **2018**, 4175–4180.

20 A. Bashir, A. H. Pandith, A. Qureashi and L. A. Malik, *New Journal of Chemistry*, 2023, **47**, 1548–1562.

21 Z. Jiang, L. Feng, J. Zhu, B. Liu, X. Li, Y. Chen and S. Khan, *Ceramics International*, 2021, **47**, 8996–9007.

22 L. A. Al-Hajji, A. A. Ismail, A. Bumajdad, M. Alsaidi, S. A. Ahmed, F. Almutawa and A. Al-Hazza, *Ceramics International*, 2020, **46**, 20155–20162.

23 S. Meng, Y. Bi, T. Yan, Y. Zhang, T. Wu, Y. Shao, D. Wei and B. Du, *Journal of Hazardous Materials*, 2018, **358**, 20–32.

24 H. Joazet Ojeda-Galván, D. Coghlan-Cárdenas, S. Eduardo Negrete-Duran, M. Ángel Vidal, J. Alanis, M. Pérez-Valverde, L. Bazan-Díaz, R. Mendoza-Cruz, Y. G. Velázquez-Galván, R. Ocampo-Pérez, M. Quintana, H. R. Navarro-Contreras and E. Giovanny Villabona-Leal, *Journal of Photochemistry and Photobiology A: Chemistry*, 2025, **459**, 116035.

25 X. Yu, Y. Mi, Z. Gong, Y. Zhang, L. Wang and S. Zeng, *ACS Applied Nano Materials*, 2024, **7**, 5156–5168.

26 T. Hu, H. Li, Z. Liang, N. Du and W. Hou, *Journal of Colloid and Interface Science*, 2019, **545**, 301–310.

27 M. Sun, Y. Kong, Y. Fang, S. Sood, Y. Yao, J. Shi and A. Umar, *Dalton Transactions*, 2017, **46**, 15727–15735.

28 S.-M. Lam, J.-C. Sin, A. Abdullah and A. Mohamed, *Chemical Papers*, 2013, **67**, 1277–1284.

29 Z. Zhang, Y. Yang and D. Cheng, *International Journal of Electrochemical Science*, 2021, **16**, 21115.

30 L. A. Al-Hajji, A. A. Ismail, M. Alsaidi, S. A. Ahmed, F. Almutawa and A. Bumajdad, *Journal of Nanoparticle Research*, 2020, **22**, 40.